Performance Assessment of Dynamic Mode Decomposition for Identifying Closely Spaced Modes in Structures

Hossein Soleimani, Ali Salehzadeh Nobari*, Hossein Hosseini-Toudeshky

Department of Aerospace Engineering, Amirkabir University of Technology, Tehran, Iran

Corresponding author, E-mail: sal1358@aut.ac.ir

Abstract:

This study evaluates the capability of standard Dynamic Mode Decomposition to identify closely spaced and nearly repeated structural modes. Two numerical benchmarks are considered: a four-degree-of-freedom mass–spring system with controlled modal spacing and a proportionally damped simply supported plate with varying aspect ratio. Natural-frequency and damping-ratio errors are quantified using the Frequency Spacing Index and Modal Overlap Factor. Robustness is further assessed by adding Gaussian measurement noise at Signal-to-Noise-Ratio levels of 90, 80, and 70 dB using 100 realizations, while the Eigensystem Realization Algorithm is employed as an independent benchmark. The results show that Dynamic Mode Decomposition can resolve very small frequency separations once an exact repeated condition is slightly perturbed. Natural-frequency estimates remain comparatively stable as modal overlap and noise increase, whereas damping-ratio estimates are more sensitive, particularly for higher-order modes. Measurement noise also reduces the maximum Modal Overlap Factor for which two closely spaced modes can be reliably separated. Under noise-free conditions, Dynamic Mode Decomposition and Eigensystem Realization Algorithm exhibit comparable resolution limits, while Eigensystem Realization Algorithm generally maintains reliable modal separation over a wider Modal Overlap Factor range as noise increases. These findings clarify the capability, sensitivity, and practical limitations of standard Dynamic Mode Decomposition for closely spaced structural modal identification.

Keywords:

Dynamic Mode Decomposition, Modal parameter identification, Closely Spaced Modes, Modal Overlap Factor, Frequency Spacing Index

1. Introduction

Closely spaced modes are frequently encountered in mechanical, aerospace, and civil structures, where their accurate identification is important for vibration analysis, resonance assessment, and structural health monitoring. Over the years, this problem has been addressed through several modal identification strategies. In output-only frameworks, Agneni and Coppotelli et al. [1] estimated modal parameters from power

ACCEPTED MANUSCRIPT

spectral density (PSD)-based frequency response function (FRF) reconstruction, Rainieri and Fabbrocino [2] examined the use of second-order blind identification (SOBI), Hosseini Kordkheili et al. [3] applied Natural Excitation Technique Eigensystem Realization Algorithm (NExT-ERA), and Wu et al. [4] improved Stochastic Subspace Identification (SSI) -based identification using stabilization procedures. Frequency-domain and probabilistic approaches have also been used, including modified Frequency Domain Decomposition (FDD) for close spectral peaks [5] and Bayesian Stochastic Subspace Identification (SSI) for large-scale structural monitoring [6]. In addition, several signal-processing-based approaches have been proposed to enhance the separation of adjacent modes, including wavelet-based methods like Generalized Intrinsic Function through Wavelet Packet Decomposition (GIFWPD) [7], modified complex Morlet wavelet function [8], continuous wavelet transform with pattern search optimization [9], or Kalman-filter-based decomposition [10], and Complex Mode Indicator Function with Singular Value Decomposition (CMIF-SVD) [11]. Other studies have examined the problem from a modal-sensitivity perspective, using perturbation theory based on Local Correspondence (LC) Principle [12], and Structural Dynamic Modification (SDM) theory [13] to investigate the behavior of closely spaced or nearly repeated modes.

Despite these developments, the reliable identification of closely spaced modes remains a challenging problem, particularly when modal frequencies approach each other and the contribution of individual modes becomes difficult to distinguish in the measured response [2]. Many existing methods also rely on specific assumptions, require additional processing steps, or may become computationally demanding for larger structural systems. This continuing challenge motivates the use of data-driven techniques capable of extracting modal information directly from structural time responses. Among these techniques, Dynamic Mode Decomposition (DMD) is particularly attractive because it provides spatial modes together with their associated temporal properties, such as frequency and damping, from time-domain data [14]. Recent studies have begun to investigate structural modes using DMD-based modal identification approaches[15]. For example, DMD combined with clustering and rank-stabilization techniques has been applied to complex wing structural models[16], while more recent studies have introduced NExT-DMD and noise-robust or variable-projection DMD formulations for Operational Modal Analysis (OMA) [17]. These studies demonstrate the potential of DMD-based approaches for modal identification and possibly separating closely spaced modes; however, their primary emphasis is generally on developing or improving the identification methodology rather than systematically characterizing the resolution capability of DMD under small controlled changes in system properties [12].

This study therefore investigates the resolution capability of standard DMD in identifying closely spaced modes and systematically examines how its performance changes as the modes progress from well-separated to closely spaced, nearly repeated, and repeated conditions. To this end, the modal spacing is

ACCEPTED MANUSCRIPT

systematically varied through controlled changes in system properties in two numerical case studies: by changing a stiffness parameter in a 4-DOF mass-spring system adopted from Ref. [13], and by modifying the aspect ratio of a simply supported plate. Both lower- and higher-order closely spaced modal pairs are considered, and the resulting errors in natural frequency and damping ratio are evaluated. The DMD results are validated against well-defined reference solutions obtained analytically for the 4-DOF system and from finite-element eigenvalue analysis and the analytical modal damping relationships for the damped plate. Although noise-free numerical data provide a controlled benchmark for isolating the effect of modal spacing, practical measurements are inevitably affected by noise; therefore, noisy data are considered to assess the robustness of DMD under more realistic conditions, with the well-established Eigensystem Realization Algorithm (ERA) used as an independent modal-identification benchmark for comparison. Since eigenvector sensitivity, especially in the presence of repeated modes, is considerably more complex and is often treated separately[18, 19], the present study mainly focuses on the identification of eigenvalues and their corresponding natural frequencies and damping ratios.

2. Theoretical Background

This section briefly summarizes the Dynamic Mode Decomposition (DMD) framework and its implementation for structural modal identification. The method was originally introduced in fluid dynamics, and detailed derivations are available in [14]. Here, the formulation is presented from a structural dynamics perspective, emphasizing the link between DMD eigenvalues and classical modal parameters.

$$\mathbf{M}\ddot{\mathbf{x}}(t) + \mathbf{C}\dot{\mathbf{x}}(t) + \mathbf{K}\mathbf{x}(t) = \mathbf{f}(t) \tag{1}$$

Where $\mathbf{b}(t) \in R^n$ is the displacement vector, $\mathbf{M} \in R^{n\times n}$ is the mass matrix, $\mathbf{C} \in R^{n\times n}$ is the damping matrix, and $\mathbf{K} \in R^{n\times n}$ is the stiffness matrix. In operational conditions, the excitation $\mathbf{f}(t)$ is typically unknown and for theoretical development of the homogeneous dynamics, the free response case $\mathbf{f}(t) = o$ is considered.

By defining a state vector

$$\mathbf{v}(t) = \begin{bmatrix} \mathbf{x}(t) \\ \dot{\mathbf{x}}(t) \end{bmatrix} \tag{2}$$

Eq. (**1**) can be rewritten in first order state space form as

$$\dot{\mathbf{v}}(t) = \mathbf{A}_c\mathbf{v}(t), \quad \mathbf{A}_c = \begin{bmatrix} 0 & \mathbf{I} \\ -\mathbf{M}^{-1}\mathbf{K} & -\mathbf{M}^{-1}\mathbf{C} \end{bmatrix} \tag{3}$$

The eigenvalues of $\mathbf{A}_c$ are directly related to modal parameters, and for the underdamped modes they can be expressed as

$$\lambda_k = -\zeta_k\omega_{n_k} \pm j\omega_{n_k}\sqrt{1-\zeta_k^2} \tag{4}$$

ACCEPTED MANUSCRIPT

Where ω_{n_k} and ζ_k represent the natural frequency and damping ratio of the mode k, respectively.

The solution to the continuous-time system is given by

$$\mathbf{v}(t) = e^{\mathbf{A}_c t}\mathbf{v}(0) \tag{5}$$

Where $\mathbf{v}(0)$ denoting the initial condition. In discrete form, the state transition over a sampling interval Δt is governed by the matrix exponential. In the free response case, the exact relationship between two consecutive time instants t_i and $t_{i+1} = t_i + \Delta t$ is

$$\mathbf{v}(t_{i+1}) = e^{\mathbf{A}_c \Delta t}\mathbf{v}(t_i) = \mathbf{A}_d \mathbf{v}(t_i), \quad \mathbf{A}_d = e^{\mathbf{A}_c \Delta t} \tag{6}$$

This relation indicates that the state transition between two consecutive time instants for homogeneous linear time invatiant (LTI) systems depends on both the sampling interval Δt and the underlying continuous-time dynamics. In practice, measured operational responses are influenced by unknown inputs and noise; DMD then estimates the best-fit linear mapping that advances the measured snapshots over the chosen time window. This means that, DMD as a data-driven technique, is designed to approximate the discrete-time evolution operator $\mathbf{A}_d$ directly from time-series measurements. The measured system response is arranged in the form of snapshot sequence in a general matrix

$$\mathbf{V}_1^N = \begin{Bmatrix} | & | & | & & | \\ \mathbf{v}_1 & \mathbf{v}_2 & \mathbf{v}_3 & \cdots & \mathbf{v}_N \\ | & | & | & & | \end{Bmatrix} \in R^{m \times N} \tag{7}$$

Where N denotes the total number of sampled time instants, and the leading dimension m is the number of measurement channels in state space representation. For example, in a 2-DOF system, if displacements and velocities are both included, then m doubles number of DOFs and equals 4 accordingly.

DMD assumes a best-fit linear mapping that connects each observation $\mathbf{v}_i$ to the subsequent one $\mathbf{v}_{i+1}$, through

$$\mathbf{v}_{i+1} = \mathbf{A}\mathbf{v}_i \tag{8}$$

Where the operator A is assumed to remain approximately constant over the sampling interval. This fundamental assumption behind DMD enables the formulation of the snapshot sequence as a Krylov subspace. By defining $\mathbf{X} = \mathbf{V}_1^{N-1}$ and $\mathbf{Y} = \mathbf{V}_2^N$, the equation of discrete dynamical system can be compactly expressed as

$$\mathbf{Y} = \mathbf{A}\mathbf{X} \tag{9}$$

The optimal linear operator A is given by the minimum norm least-squares solution

ACCEPTED MANUSCRIPT

$$\mathbf{A} = \mathbf{Y}\mathbf{X}^{\dagger} \tag{10}$$

Where $\mathbf{X}^{\dagger}$ denotes the Moore-Penrose pseudoinverse of $\mathbf{X}$.

While inversing a high-dimensional matrix brings difficulties, DMD projects the dynamics onto a reduced subspace obtained from taking singular value decomposition (SVD) of $\mathbf{X} = \mathbf{U}\mathbf{\Sigma}\mathbf{V}^{*}$, allowing a reduced estimation of A.

$$\tilde{\mathbf{A}} = \mathbf{U}^{*}\mathbf{A}\mathbf{U} = \mathbf{U}_r^{*}\mathbf{Y}\mathbf{V}_r\mathbf{\Sigma}_r^{-1} \tag{11}$$

Where r is optimal rank of the SVD and truncation is based on it to obtain $\mathbf{U}_r$, $\mathbf{\Sigma}_r$ and $\mathbf{V}_r$.

By assuming $\tilde{\mathbf{A}} \approx \mathbf{A}_d$, the reduced operator eigenvalues (μ_k), commonly referred to as the system poles, are related to the continuous-time modal parameters through

$$\lambda_k = \frac{\ln(\mu_k)}{\Delta t} = -\zeta_k \omega_{n_k} \pm j\omega_{n_k}\sqrt{1-\zeta_k^2} \tag{12}$$

This formulation highlights that the temporal evolution of the measured data inherently follows an exponential behavior, originating from the solution of the underlying continuous-time LTI system. The corresponding DMD modes in the measurement space are

$$\Phi_k = \mathbf{Y}\mathbf{V}_r\mathbf{\Sigma}_r^{-1}\Psi_k \tag{13}$$

Where Ψ_k is the eigenvector of $\tilde{\mathbf{A}}$ for mode k and Φ_k is its representation in measurement state space. Along with eigenvalues and modes, DMD also yields modal amplitudes that scale the contribution of each mode in reconstructing the snapshot matrix $\mathbf{V}_1^N$ [20]. However, reconstruction is not the objective here, and the analysis focuses instead on extracting natural frequencies and damping ratios reliably from the DMD eigenvalues.

Besides reducing the data dimension, truncation to rank r can also suppress the noise floor spatially by discarding low-energy components that are typically dominated by measurement noise. It should be noted that the number of identifiable modes is practically limited by the optimal rank used in the SVD projection. The standard DMD procedure in [14] is adopted here to find structural modal parameters.

Algorithm: Standard DMD

1. Stack all m channels over N time instants to form the snapshot matrix $\mathbf{V}_1^N \in R^{m\times N}$
2. Form matrices $\mathbf{X}$ and $\mathbf{Y}$ from the original dataset $\mathbf{V}_1^N$ and take SVD of $\mathbf{X}$, letting $\mathbf{X} = \mathbf{U}\mathbf{\Sigma}\mathbf{V}^{*}$
3. Apply truncation based on optimal rank of SVD singular values to obtain $\mathbf{U}_r$, $\mathbf{\Sigma}_r$ and $\mathbf{V}_r$.
4. Let define $\tilde{\mathbf{A}} = \mathbf{U}^{*}\mathbf{A}\mathbf{U} = \mathbf{U}_r^{*}\mathbf{Y}\mathbf{V}_r\mathbf{\Sigma}_r^{-1}$

ACCEPTED MANUSCRIPT

5. Find the eigenvalues μ_k and eigenvectors Φ_k of $\tilde{\mathbf{A}}$ with $\tilde{\mathbf{A}}\Psi_k = \mu_k \Psi_k$

6. By adopting modal coordinates, eigenvalues of a vibrational system are obtained by $\lambda_k = \dfrac{\ln(\mu_k)}{\Delta t}$

   where $\lambda_k = -\zeta_k \omega_{n_k} \pm j\omega_{n_k}\sqrt{1-\zeta_k^2}$

7. And finally, frequency and damping ratio are obtained by $\omega_{n_k} = \dfrac{|\lambda_k|}{2\pi}$ and $\zeta_k = \dfrac{-real(\lambda_k)}{|\lambda_k|}$

when the number of measurement channels is limited (small m), the snapshot matrices can be augmented using a Hankel shift-stacking embedding approach [21, 22]. The number of columns in $\mathbf{V}_1^N$ is the number of snapshots and indicate temporal dimension of dataset. For undamped dynamical systems, the presence of one or two oscillations in the response of all measurement points are enough to identify natural frequencies. The number of rows in $\mathbf{V}_1^N$ indicates spatial dimension and it can be truncated by two techniques: reducing number of measurement points or truncating dataset by Singular Value Decomposition (SVD).

To provide an independent benchmark for evaluating the modal-resolution capability of DMD, the Eigensystem Realization Algorithm (ERA), a well-established time-domain modal identification method, was also applied to the plate responses. ERA was used only as a comparative identification method and not as the ground-truth reference. The same acceleration and velocity response records, sampling frequency, and data length used for DMD were employed in the ERA analysis.

Using the state vectors $\mathbf{v}_k$ already defined in Eq. (**2**), two block-Hankel matrices shifted by one sampling interval are constructed as [23]

$$\mathbf{H}_0 = \begin{bmatrix} \mathbf{v}_1 & \mathbf{v}_2 & \cdots & \mathbf{v}_j \\ \mathbf{v}_2 & \mathbf{v}_3 & \cdots & \mathbf{v}_{j+1} \\ \vdots & \vdots & \ddots & \vdots \\ \mathbf{v}_i & \mathbf{v}_{i+1} & \cdots & \mathbf{v}_{i+j-1} \end{bmatrix}, \quad \mathbf{H}_1 = \begin{bmatrix} \mathbf{v}_2 & \mathbf{v}_3 & \cdots & \mathbf{v}_{j+1} \\ \mathbf{v}_3 & \mathbf{v}_4 & \cdots & \mathbf{v}_{j+2} \\ \vdots & \vdots & \ddots & \vdots \\ \mathbf{v}_{i+1} & \mathbf{v}_{i+2} & \cdots & \mathbf{v}_{i+j} \end{bmatrix} \tag{14}$$

A reduced-order realization is obtained from the singular value decomposition of $\mathbf{H}_0$,

$$\mathbf{H}_0 = \mathbf{U}\boldsymbol{\Sigma}\mathbf{V}^T, \quad \mathbf{A}_{ERA} = \boldsymbol{\Sigma}_r^{-1/2}\mathbf{U}_r^T\mathbf{H}_1\mathbf{V}_r\boldsymbol{\Sigma}_r^{-1/2} \tag{15}$$

The corresponding output matrix and modal eigensystem are

$$\mathbf{C}_{ERA} = \mathbf{E}_m^T\mathbf{U}_r\boldsymbol{\Sigma}_r^{-1/2}, \quad \mathbf{A}_{ERA}\Psi = \Psi\Lambda, \quad \Phi_{ERA} = \mathbf{C}_{ERA}\Psi \tag{16}$$

ACCEPTED MANUSCRIPT

Where $\mathbf{E}_m^T = [\mathbf{I}_m \quad 0 \quad \dots \quad 0]$. The eigenvalues in λ are converted to continuous-time modal parameters using the same logarithmic relation introduced previously for DMD in Eq. (**12**). The columns of Φ_{ERA} provide the corresponding mode shapes at the measurement locations.

To quantitatively describe the closeness of two modes, several measures have been used in the literature, most of which are based on the frequency separation between adjacent modes. For damped systems, a commonly used index is the Modal Overlap Factor (MOF), which accounts for both modal spacing and damping. For two adjacent modes, it can be expressed as

$$\delta_k = \frac{\omega_{n_k} \zeta_k}{\left(\omega_{n_k} - \omega_{n_{k-1}}\right)} \tag{17}$$

Where ω_{n_k} and ζ_k denote the natural frequency and damping ratio of the kth mode, respectively[3]. A larger MOF indicates a greater degree of modal overlap; therefore, repeated modes theoretically lead to an unbounded MOF. Hosseini Kordkheili et al.[3], used this index in their study of closely spaced modes identified by NExT-ERA and noted that modes with MOF values greater than 0.17 may be regarded as moderately close. In their numerical and experimental examples, MOF values around 0.31–0.32 were reported for close modal pairs, indicating a higher degree of modal closeness. It should be noted, however, that such threshold values are problem-dependent and should not be interpreted as universal limits.

For numerical examples like a four-DOF mass-spring system presented in[24], MOF value of 0.01 is considered to have well separated modes and MOF value of 0.1 means that the modes are closely spaced. It should be emphasized that MOF is not a purely frequency-based measure of modal closeness, since it depends directly on the modal damping ratio. Therefore, two modal pairs with the same frequency separation may have different MOF values if their damping ratios are different. In this sense, MOF is more appropriately interpreted as a measure of damping-dependent modal overlap, whereas a frequency-spacing measure such as FSI provides a damping-independent description of the spectral proximity of two modes.

An alternative measure was used by Jonscher et al.[6], who defined a close mode factor based on the normalized frequency distance relative to the modal half-power bandwidth. This factor behaves inversely to the MOF: it tends to zero for repeated modes and increases as the modal frequencies become more separated. For repeated modes MOF tends to infinity while close mode factor tends to zero.

To characterize the frequency proximity for undamped systems, modal closeness can be quantified using a frequency spacing index (FSI) based only on the relative difference between two adjacent natural frequencies:

ACCEPTED MANUSCRIPT

$$\gamma_k = \frac{2\left(\omega_{n_k} - \omega_{n_{k-1}}\right)}{\omega_{n_k} + \omega_{n_{k-1}}}$$

This index is usually reported as a percentage and tends to zero as the modes approach a repeated-eigenvalue condition. Accordingly, FSI is particularly useful for distinguishing the intrinsic frequency proximity of well-separated, closely spaced, nearly repeated, and repeated modes without the influence of damping. Wu et al.[4], used this type of index to evaluate closely spaced modes in civil structures and reported that their upgraded SSI methodology could identify extremely close modes with a frequency spacing index on the order of 0.1%. Reviewing the literature indicates that only a limited number of studies have reported successful identification at extremely small frequency-spacing beyond the level of $\gamma = 0.1\%$ for numerical cases and $\gamma = 1\%$ for testing models or real structures[4]. In the present study, FSI is used as a damping-independent measure of frequency proximity, whereas MOF is employed for the damped cases to quantify the combined effect of frequency spacing and damping on modal overlap. Thus, FSI characterizes how close the modal frequencies are, while MOF provides a complementary measure of the severity of modal overlap and the associated identification difficulty. Both MOF and FSI are dimensionless ratios and they have the same numerical values whether natural frequencies in $^{rad}/_{s}$ or Hz is used, provided that the same frequency unit is used consistently throughout each formula.

3. Case Studies

3-1- Discrete 4-DOF System

A four-degree-of-freedom (DOF) mass-spring system, adopted from Ref [13], is first considered to evaluate the sensitivity of standard DMD to small stiffness variations and to examine its ability to identify closely spaced modes. The configuration of the system, together with the corresponding mass and stiffness parameters, is shown in Fig. 1 For each stiffness value, a free-vibration time-history analysis is performed by applying an initial displacement to the system. The resulting acceleration and velocity responses are then sampled at uniform time intervals and used as the input data for the DMD analysis.

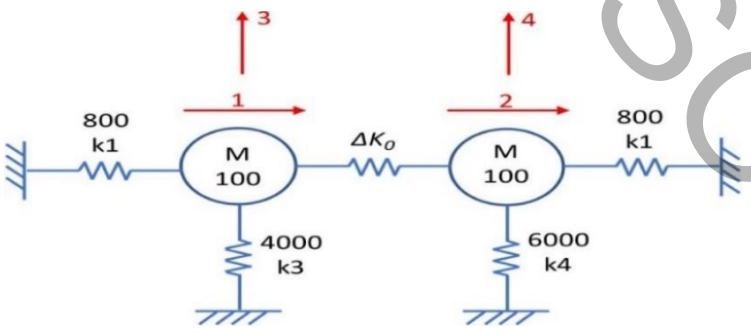


Fig. 1: A four DOF's mass/spring System

The stiffness and mass matrix of the system are defined as

ACCEPTED MANUSCRIPT

$$\mathbf{K} = \begin{bmatrix} 800 & 0 & 0 & 0 \\ 0 & 800 & 0 & 0 \\ 0 & 0 & 4000 & 0 \\ 0 & 0 & 0 & 6000 \end{bmatrix} + \begin{bmatrix} \Delta K_0 & -\Delta K_0 & 0 & 0 \\ -\Delta K_0 & \Delta K_0 & 0 & 0 \\ 0 & 0 & 0 & 0 \\ 0 & 0 & 0 & 0 \end{bmatrix} \quad 19$$

$$\mathbf{M} = \begin{bmatrix} 100 & 0 & 0 & 0 \\ 0 & 100 & 0 & 0 \\ 0 & 0 & 100 & 0 \\ 0 & 0 & 0 & 100 \end{bmatrix} \quad 20$$

A relatively large value of the stiffness parameter ΔK_0 leads to well-separated modes, whereas reducing this parameter gradually decreases the spacing between the first two natural frequencies. In the limiting case of ΔK_0, the two modes become repeated. For each value of ΔK_0, the free response of the system is computed over a duration of 3 s by imposing an initial displacement at $t = 0\text{s}$. The acceleration and velocity time histories of all four DOFs are then used to form the state snapshots for DMD, from which the first two natural frequencies are estimated. Fig. 2 shows the acceleration responses of the four DOFs for the mass-spring system. Although one or two response cycles are often sufficient for frequency identification in undamped systems, approximately four cycles are retained in this study to improve the reliability of the DMD estimates.

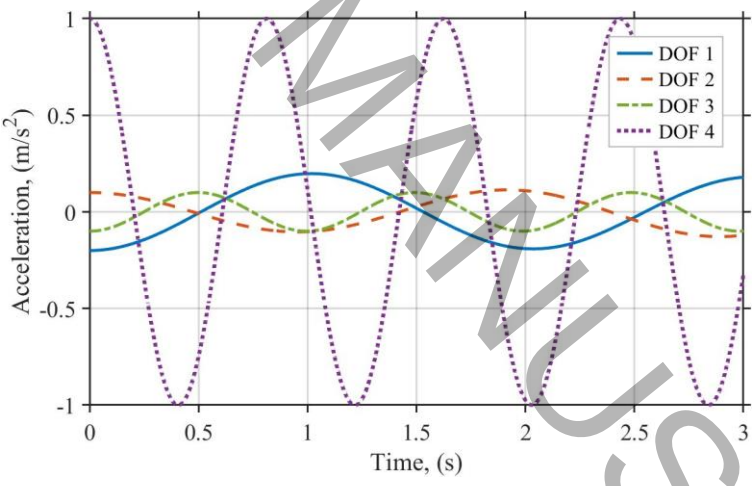


Fig. 2: Acceleration response of undamped mass/spring system to initial displacement

Fig. 3 compares the squared natural frequencies estimated by DMD with the exact eigenvalues as a function of FSI. As the FSI decreases, the first two modes gradually approach each other and the identification problem becomes increasingly demanding. DMD remains able to identify the two nearly repeated modes with good agreement with the exact solution down to an FSI of approximately $\gamma = 0.013\%$. At still smaller frequency spacing, the first natural frequency remains accurately captured, whereas the estimation of the second natural frequency begins to deviate. This level of modal spacing is smaller than the resolution levels reported for many conventional identification methods in the literature [13]. Although the sensitivity of

ACCEPTED MANUSCRIPT

eigenvalues to system changes has been discussed in previous studies [18, 19], the identification of closely spaced modes in the range of $\gamma < 0.1\%$ has rarely been examined in detail [8].

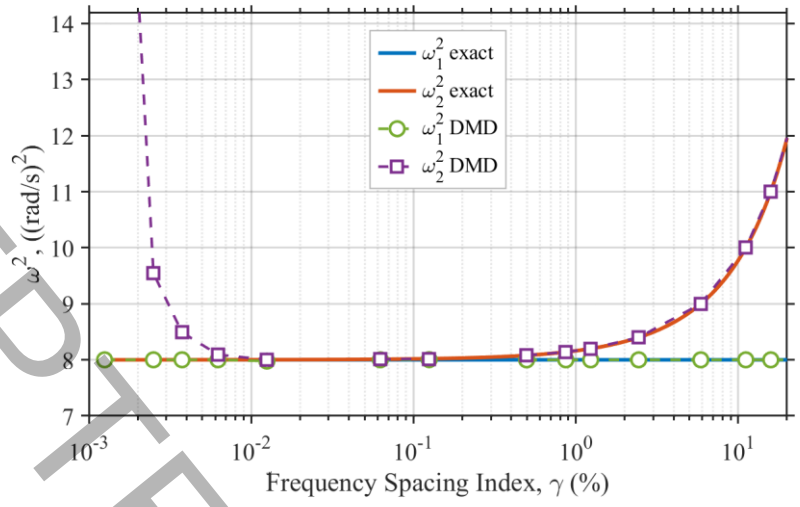


Fig. 3: DMD and exact eigenvalues of the first two modes versus frequency spacing index

The sensitivity analysis in Ref. [13] was limited to an undamped mass-spring system. To examine the performance of DMD under damped conditions, viscous dampers are added to the 4-DOF system, as shown in Fig. 4. The damping coefficients are selected such that all modes remain underdamped, allowing the natural frequencies and damping ratios to be extracted from the time-response data.

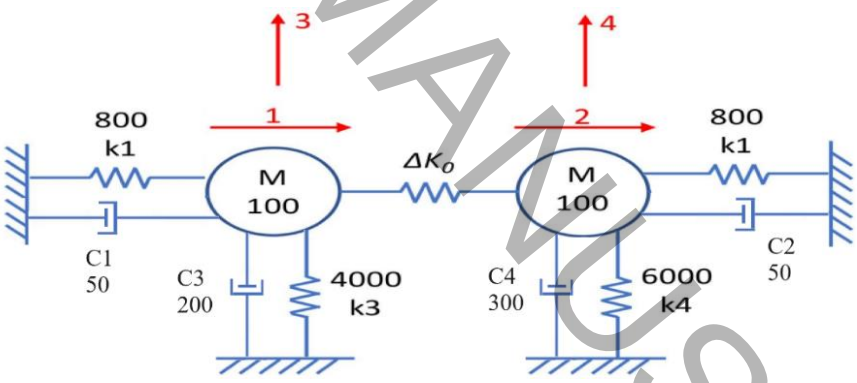


Fig. 4: The proposed 4 DOF system with viscous damping

The viscous damping matrix of the 4-DOF system is defined as

$$\mathbf{C} = \begin{bmatrix} 50 & 0 & 0 & 0 \\ 0 & 50 & 0 & 0 \\ 0 & 0 & 200 & 0 \\ 0 & 0 & 0 & 300 \end{bmatrix} \tag{21}$$

Using the selected damping arrangement, the system remains underdamped and the damping ratios can be obtained through modal transformation. The undamped eigenvectors are collected in the modal matrix, and

ACCEPTED MANUSCRIPT

the physical mass, stiffness, and damping matrices are transformed into the modal coordinates. Since the resulting modal damping matrix is diagonal for the present system, the damping ratios are calculated as in Eq. (**22**)

$$[\zeta]=\frac{1}{2}\left([\Phi]^T[\mathbf{M}][\Phi]\right)^{-1}\left([\Phi]^T[\mathbf{C}][\Phi]\right)\left([\omega_n]\right)^{-1} \tag{22}$$

Where $[\Phi]$ is the matrix of undamped mode shapes or eigenvectors, and $[\omega_n]$ is the diagonal matrix of undamped natural frequencies [25]. For the selected mass and damping values, the damping ratios are inversely proportional to the natural frequencies, as expressed in Eq. (**23**).

$$[\zeta]=\begin{bmatrix} \frac{1}{4\omega_{n1}} & 0 & 0 & 0 \\ 0 & \frac{1}{4\omega_{n2}} & 0 & 0 \\ 0 & 0 & \frac{1}{\omega_{n3}} & 0 \\ 0 & 0 & 0 & \frac{1}{\omega_{n4}} \end{bmatrix} \tag{23}$$

Fig. 5 shows the free-decay acceleration responses of the damped 4-DOF system over a duration of 3 s, obtained after applying an arbitrary initial load. Although the excitation is not explicitly included in the standard DMD formulation, it should provide sufficient modal content in the measured responses so that the modes of interest can be identified from the resulting snapshot data [26].

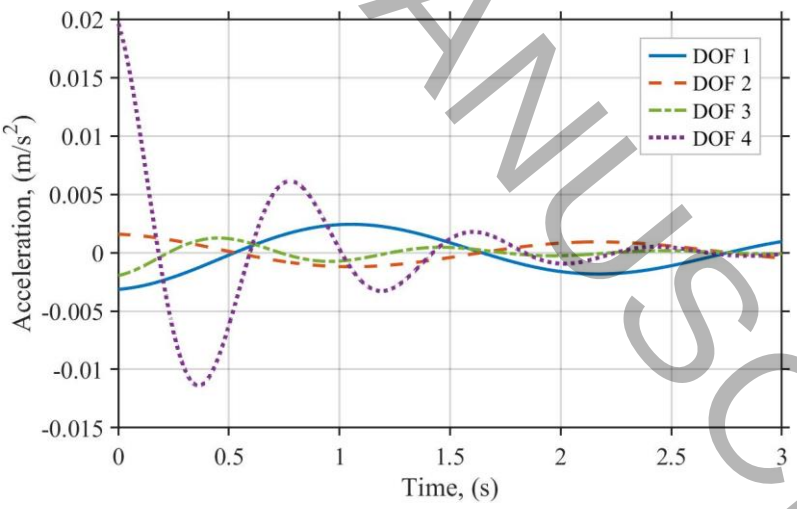


Fig. 5: Acceleration response of viscously damped system to initial displacement

Fig. 6 compares the squared natural frequencies estimated by DMD with the exact eigenvalues of the damped system as a function of the Modal Overlap Factor (MOF). As the MOF increases, the two modes become progressively more overlapped and the identification problem becomes more demanding. The

ACCEPTED MANUSCRIPT

results show that DMD remains capable of accurately resolving the two modes over a relatively high range of MOF values, with the estimated eigenvalues closely following the exact solutions $(MOF \leq 70)$. However, beyond a certain level of modal overlap, the estimate of the second mode begins to deviate noticeably, while the first mode remains accurately identified. This behavior indicates the existence of a practical resolution threshold for standard DMD in the present damped system. Compared with the undamped case, viscous damping reduces the range over which two very closely spaced modes can be reliably separated.

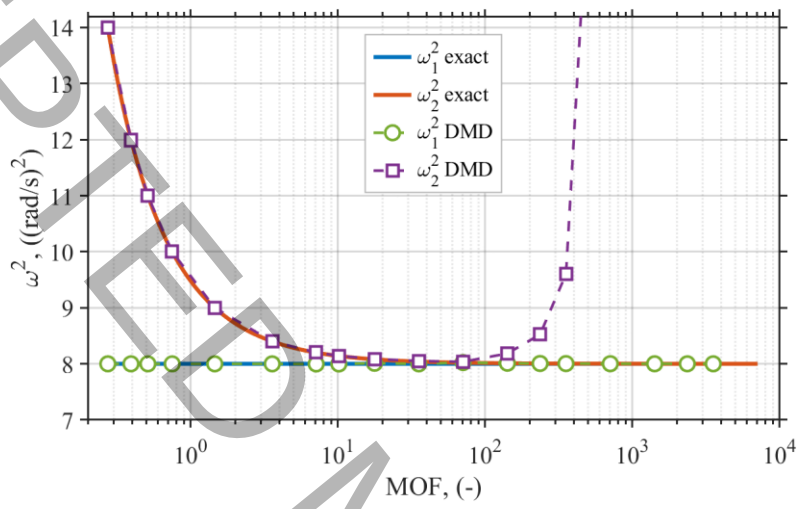


Fig. 6: Variation of the first two natural frequencies of the damped system

Fig. 7 shows the damping ratios estimated by DMD with the analytical values for the first two modes as a function of MOF. At low and moderate MOF values $(MOF \leq 20)$, the DMD estimates remain in good agreement with the analytical damping ratios. As the modal overlap increases and the two modes become more difficult to distinguish, the damping-ratio estimate of the second mode begins to deviate noticeably from the reference value, while the first mode remains comparatively stable. This behavior confirms that damping estimation is more sensitive to increasing modal overlap than frequency estimation and indicates a lower practical resolution limit for damping identification in the present damped system.

ACCEPTED MANUSCRIPT

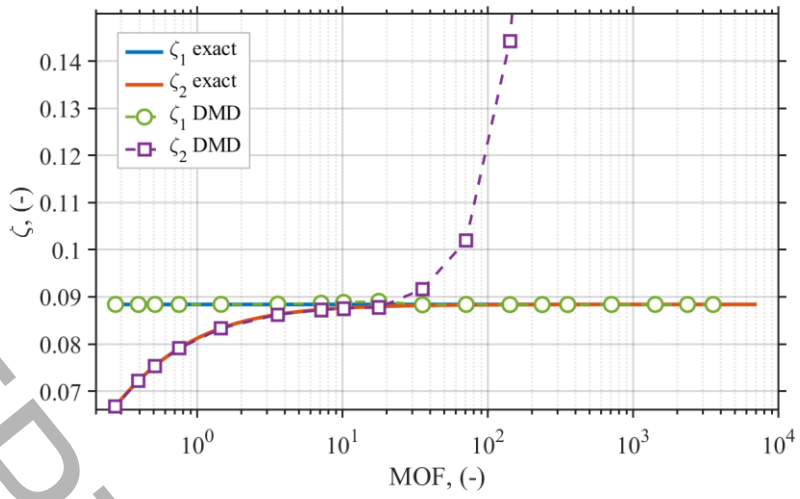


Fig. 7: Variation of the first two damping ratios of the damped system

The results of this case study show that DMD provides more reliable estimates of natural frequencies than damping ratios as modal overlap increases in damped systems. The frequency estimates remain accurate over a wider range of MOF values, whereas the damping ratio estimates begin to deteriorate at lower levels of modal overlap. It is also observed that standard DMD can resolve very closely spaced or nearly repeated modes when a small separation exists between their eigenvalues. However, in the exact repeated-eigenvalue case, the method does not separate two independent modes associated with a single temporal eigenvalue.

An additional mode-shape examination was performed for the exact repeated condition $(\Delta K = 0)$. In this case, the first two modes span a two-dimensional eigenspace associated with the same temporal eigenvalue. DMD identifies only one temporal mode from a single free-response realization, while its corresponding spatial mode remains within the analytical repeated-mode eigenspace and depends on the initial excitation. Therefore, the identified DMD mode shape should not be interpreted as a unique individual mode of the repeated pair, but rather as an excitation-dependent direction within their common eigenspace.

As an additional practical assessment, the influence of measurement noise on the DMD estimates was also examined. Random Gaussian noise was added to the numerical response channels at different signal-to-noise ratio (SNR) levels, and the DMD analysis was repeated over multiple noise realizations for each SNR level. The median estimates obtained from the ensemble are presented in Fig. 8 alongside the exact solution and the noise-free DMD results. This comparison illustrates how the identification of the first two natural frequencies changes with increasing modal overlap under noisy conditions.

ACCEPTED MANUSCRIPT

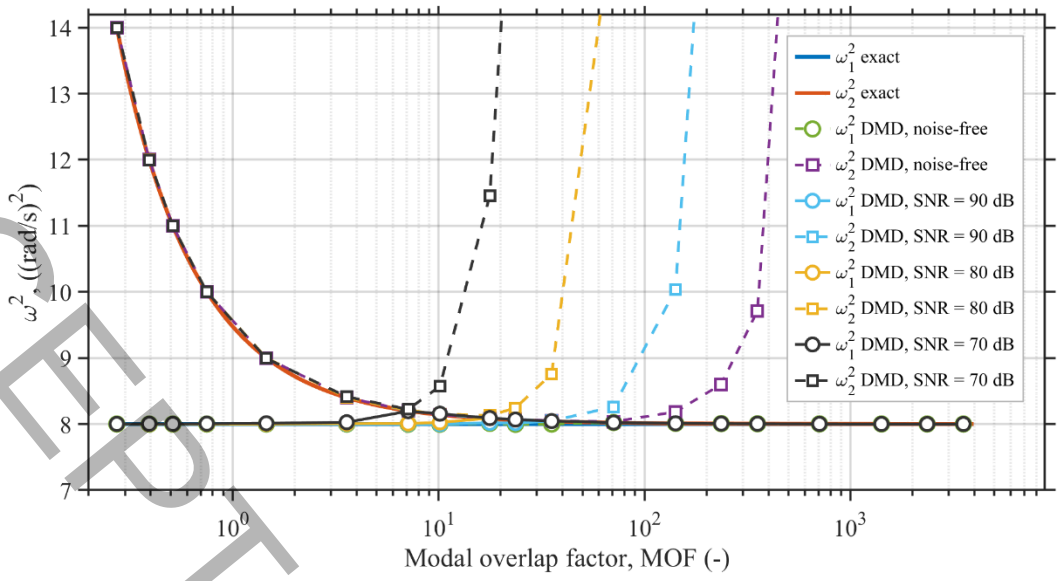


Fig. 8: Noise effect on DMD identification of the first two natural frequencies

The corresponding effect of measurement noise on the estimated damping ratios is shown in Fig. 9. Compared with the natural-frequency estimates, the damping estimates exhibit a noticeably greater sensitivity to both measurement noise and increasing modal overlap. It is also observed that, in the MOF range where the second-mode damping estimate begins to deviate, the first-mode estimate also exhibits a temporary deviation before stabilizing again at higher MOF values. In general, the deviations become more pronounced as the SNR decreases and the modes become more closely spaced.

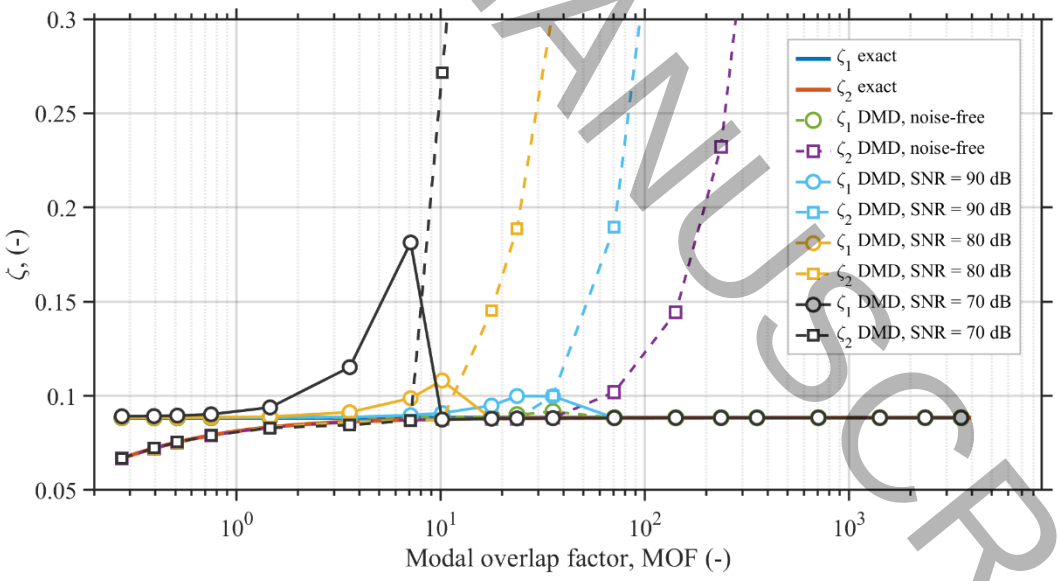


Fig. 9: Noise effect on DMD identification of the first two damping ratios

Overall, increasing measurement noise reduces the ability of DMD to distinguish closely spaced modes, with a more pronounced deterioration in damping-ratio estimation than in natural-frequency estimation.

ACCEPTED MANUSCRIPT

3-2- A Simply-Supported Plate

A simply supported steel plate is considered as the second case study to examine the performance of standard DMD for a continuous structural system. The plate has an initial square geometry with dimensions $400\text{mm} \times 400\text{mm}$ and a thickness of 1mm, and is simply supported along all four edges, as shown in Fig. 10. Its material properties were characterized by a Young's modulus of 200GPa, a density of $7800\ {}^{\text{kg}}/_{\text{m}^3}$, and a Poisson's ratio of 0.33. To control the spacing between closely spaced modes, the aspect ratio of the plate is varied in the range $1 \le {}^{b}/_{a} \le 1.25$ by increasing b from 400mm to 500mm, while keeping $a = 400\text{mm}$ constant. In this case study, the Modal Overlap Factor is used to quantify the degree of modal closeness. For the square plate, i.e., $a = b = 400\text{mm}$, modes 2 and 3 form a repeated modal pair. A similar repeated condition also occurs for modes 5 and 6, which makes this example suitable for examining the identification of closely spaced higher-order modes.

A finite element model of the plate was developed using 3D eight-node shell elements and discretized with an element size of 20mm. An eigenvalue analysis was first performed to obtain a primary numerical reference for the natural frequencies and mode shapes. A mesh-convergence study confirmed that the first six natural frequencies were converged for the selected element size. Subsequently, a dynamic implicit analysis was performed using the same finite element model to obtain the time-domain response to an initial load. The transverse acceleration and velocity responses were recorded at equally spaced measurement points, as indicated in Fig. 10. A minimum of 81 measurement points (9×9) was distributed over the plate, increasing to 90 points (9×10) for larger aspect ratios, providing sufficient spatial sampling to capture the spatial characteristics of modes 5 and 6 and avoid insufficient spatial dimensionality in DMD. A detailed investigation of the optimal number and placement of measurement points is beyond the scope of this paper.

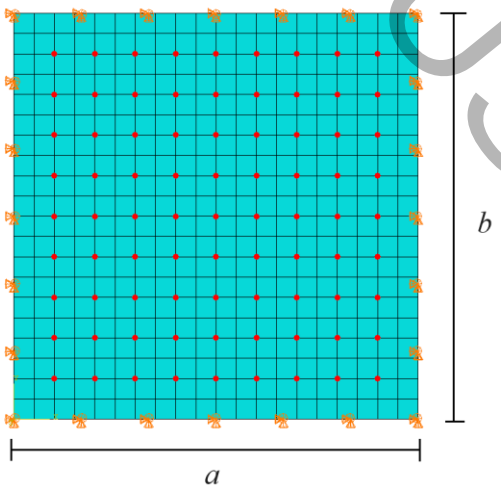


Fig. 10: 4-Edge Simply Supported Plate with mesh grid

ACCEPTED MANUSCRIPT

Proportional damping (Rayleigh) was assumed for the plate as

$$\mathbf{C} = \alpha\mathbf{M} + \beta\mathbf{K} \tag{24}$$

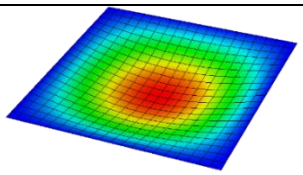
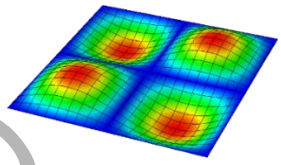
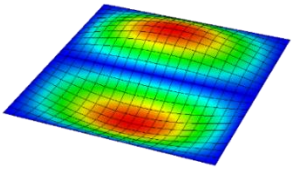
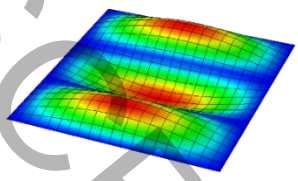
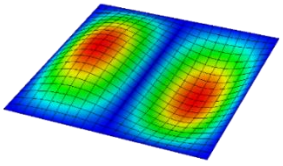
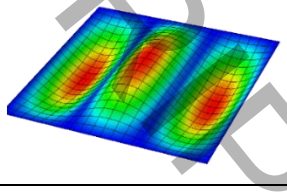
Where $\alpha = 2$ and $\beta = 3e-4$. Damping ratios are calculated using the formula

$$\zeta_k = \frac{\alpha}{2\omega_{n_k}} + \frac{\beta\omega_{n_k}}{2} \tag{25}$$

where ω_{n_k} refers to natural frequency and ζ_k is the damping ratio for mode k. The Rayleigh damping coefficients were selected to produce approximately 3% damping in the first mode, providing a representative effective structural damping level and a sufficiently observable decay rate for modal identification. Moreover, the proportional damping model provides analytically known reference damping ratios through Eq. (**25**), enabling direct quantitative evaluation of the DMD estimates.

Table 1 shows modal information for the first six modes of a nearly square four-edge simply supported plate with dimensions $400\text{mm} \times 400.5\text{mm}$, together with their corresponding natural frequencies and damping ratios. As expected for a square or nearly square plate, modes 2 and 3 form a closely spaced pair with opposite spatial orientations. A similar behavior is observed for modes 5 and 6, which represent higher-order closely spaced modes. The latter pair is particularly important in the present study, since several previous investigations on closely spaced modes have mainly examined lower-order modal pairs. Therefore, modes 5 and 6 provide a useful benchmark for examining whether standard DMD can distinguish closely spaced modes that occur at higher modal orders.

Table 1: Modal information of the plate

Mode	f_n (Hz)	ζ (−)	**Mode shape**	**Mode**	f_n (Hz)	ζ (−)	**Mode shape**
1	30.33	0.0338		4	121.34	0.1157	
2	75.81	0.0735		5	151.62	0.1439	
3	75.92	0.0736		6	151.92	0.1442	

ACCEPTED MANUSCRIPT

Table 2 presents the variation in the closeness of the second and third modes for different plate aspect ratios. For the square plate, these two modes form a repeated pair with identical natural frequencies and damping ratios, and the MOF theoretically tends to infinity. A slight increase in the aspect ratio separates the two frequencies, but the modes remain highly overlapped; for example, at $b/a = 1.001$, the frequency difference is only about 0.11Hz, while the MOF reaches 49. As the aspect ratio increases further, the second natural frequency decreases more rapidly than the third one, leading to a gradual reduction in modal overlap. Therefore, this set of cases provides a controlled benchmark for assessing the ability of standard DMD to identify closely spaced modes over a wide range of modal-overlap conditions, from nearly repeated modes to less strongly coupled modal pairs.

Table 2: Closeness of the second and third modes for different plate aspect ratios

Plate Dimension	$\frac{b}{a}$	f_2 (Hz)	f_3 (Hz)	ζ_2	ζ_3	MOF δ_3
400mm × 400mm	1	75.96	75.96	0.0737	0.0737	∞
400mm × 400.5mm	1.001	75.81	75.92	0.0735	0.0736	49
400mm × 401mm	1.003	75.65	75.88	0.0734	0.0736	24.6
400mm × 402mm	1.005	75.35	75.81	0.0731	0.0735	12.1
400mm × 404mm	1.01	74.76	75.66	0.0726	0.0734	6.2
400mm × 406mm	1.015	74.17	75.51	0.0720	0.0733	4.1
400mm × 408mm	1.02	73.6	75.37	0.0715	0.0731	3.1
400mm × 410mm	1.025	73.03	75.23	0.0710	0.0730	2.5
400mm × 420mm	1.05	70.31	74.55	0.0685	0.0724	1.3
400mm × 430mm	1.075	67.77	73.92	0.0662	0.0718	0.9
400mm × 440mm	1.1	65.41	73.33	0.0641	0.0713	0.7
400mm × 450mm	1.125	63.20	72.78	0.0621	0.0708	0.54
400mm × 460mm	1.15	61.13	72.26	0.0602	0.0703	0.46
400mm × 500mm	1.25	54.08	70.51	0.0539	0.0687	0.3

Similarly, Table 3 summarizes the modal information of the fifth and sixth modes for different plate aspect ratios. This modal pair represents a higher-order repeated or closely spaced pair and provides a more demanding benchmark than the second and third modes. For the square plate, the fifth and sixth modes have identical natural frequencies and damping ratios, and the MOF theoretically tends to infinity. With a slight increase in the aspect ratio, the repeated condition is removed, but the two modes remain strongly overlapped. For example, at $b/a = 1.001$, the frequency difference is only about 0.30Hz, while the MOF

ACCEPTED MANUSCRIPT

reaches 73, which is larger than the corresponding value for the second and third modes. As the aspect ratio increases, the fifth natural frequency decreases more rapidly than the sixth one, and the MOF gradually decreases from 73 to about 0.5. Therefore, this case extends the assessment beyond the lower-order modal pairs commonly used in closely spaced mode identification studies and provides a stricter test for the resolution capability of standard DMD.

Table 3: Closeness of the fifth and sixth modes for different plate aspect ratios

Plate Dimension	$\frac{b}{a}$	f_5 (Hz)	f_6 (Hz)	ζ_5	ζ_6	δ_6
400mm×400mm	1	151.96	151.96	0.1443	0.1443	∞
400mm×400.5mm	1.001	151.62	151.92	0.1439	0.1442	73
400mm×401mm	1.003	151.28	151.88	0.1436	0.1442	36.5
400mm×402mm	1.005	150.6	151.81	0.1430	0.1441	18.1
400mm×404mm	1.01	149.26	151.66	0.1417	0.1440	9.1
400mm×406mm	1.015	147.95	151.52	0.1405	0.1439	6.1
400mm×408mm	1.02	146.65	151.37	0.1393	0.1437	4.6
400mm×410mm	1.025	145.37	151.23	0.1381	0.1436	3.7
400mm×420mm	1.05	139.24	150.55	0.1324	0.1429	1.9
400mm×430mm	1.075	133.54	149.92	0.1270	0.1424	1.3
400mm×440mm	1.1	128.22	149.33	0.1221	0.1418	1.0
400mm×450mm	1.125	123.25	148.78	0.1175	0.1413	0.8
400mm×460mm	1.15	118.6	148.27	0.1131	0.1408	0.7
400mm×500mm	1.25	102.7	146.51	0.0984	0.1390	0.5

To obtain the acceleration and velocity responses required for DMD, a spatially asymmetric initial load is applied to the plate at $t = 0\text{s}$ to excite all modes, followed by free vibration for 0.5s. Fig. 11 shows the transverse acceleration responses recorded at four representative measurement points on the plate.

ACCEPTED MANUSCRIPT

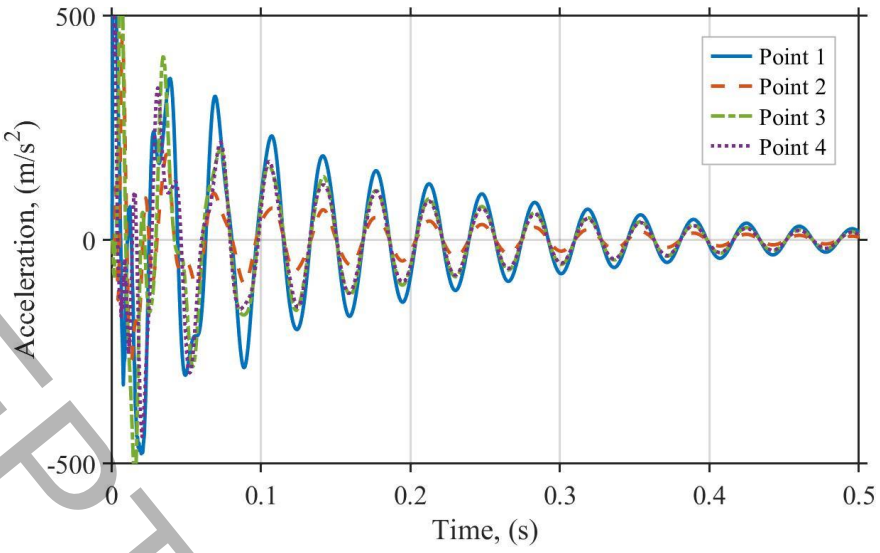
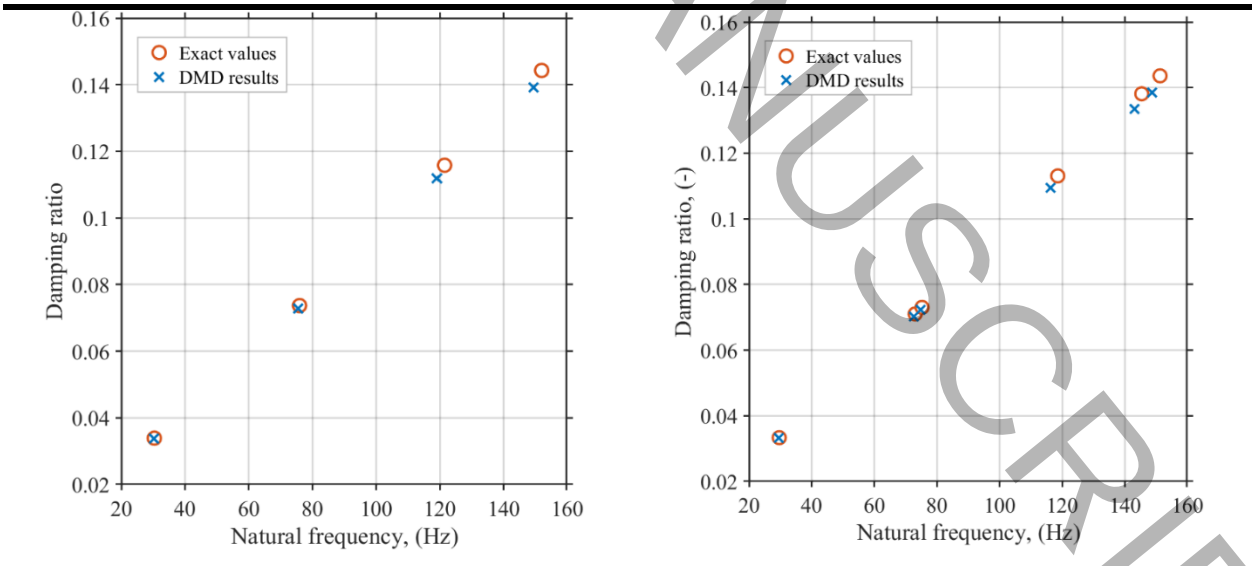


Fig. 11: Acceleration responses at five representative measurement points on the plate

Fig. 12 compares the modal parameters estimated by DMD with the reference values for the first six modes of the plate at four different aspect ratios. For the square plate, shown in Fig. 12(a), modes 2 and 3 form an exactly repeated pair. DMD therefore identifies a single temporal eigenvalue at the repeated frequency rather than two independently distinguishable modes. The same behavior is observed for the repeated modes 5 and 6. As discussed previously, the corresponding DMD spatial mode represents an excitation-dependent direction within the repeated-mode eigenspace and should not be uniquely assigned to either individual mode. As the aspect ratio increases and the repeated modes split into closely spaced pairs, DMD becomes more effective in separating the adjacent modes, as shown in Fig. 12(b-d).



ACCEPTED MANUSCRIPT

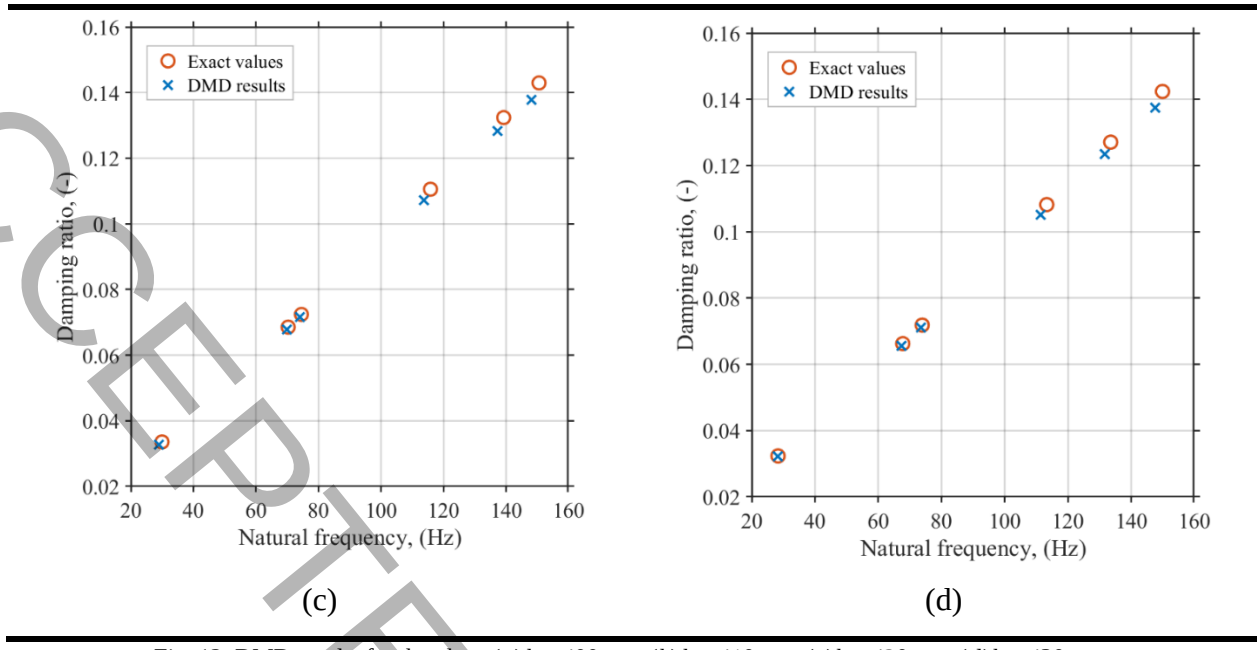


Fig. 12: DMD results for the plate $(a)b = 400\text{mm}$, $(b)b = 410\text{mm}$, $(c)b = 420\text{mm}$, $(d)b = 430\text{mm}$

Fig. 13 compares the natural frequencies estimated by DMD with the reference eigenvalue solution for modes 2 and 3 as a function of MOF. Except for the square plate, where the two modes are repeated and only one eigenvalue is identified by DMD, the two natural frequencies are accurately captured over the considered range of MOF values. The frequency errors remain below 1%, indicating that standard DMD can resolve this closely spaced modal pair once a small separation exists between the repeated modes.

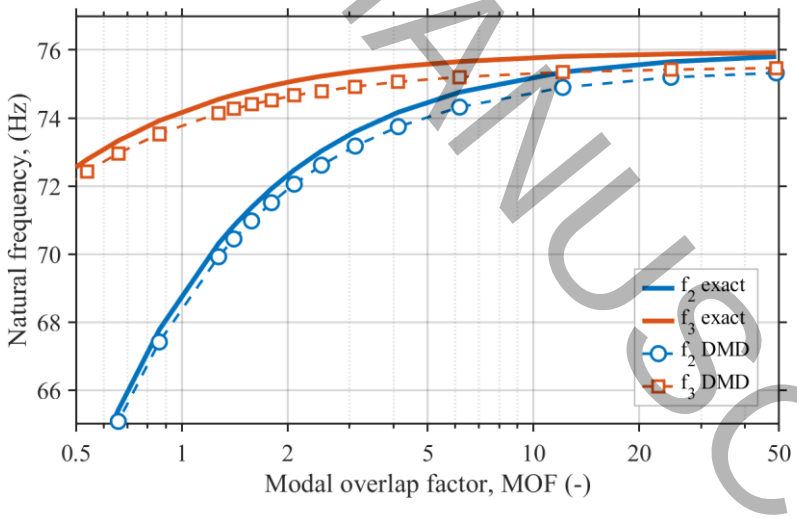


Fig. 13: DMD and reference natural frequencies of modes 2 and 3 versus MOF

Fig. 14 compares the damping ratios estimated by DMD with the reference values for modes 2 and 3 as a function of MOF. For finite MOF values, DMD successfully identifies the damping ratios of both modes over the entire investigated range. As the modal overlap increases, the reference damping ratios approach each other, while the DMD estimates continue to follow the corresponding trends with relatively small

ACCEPTED MANUSCRIPT

deviations. The discrepancy becomes more noticeable at the highest MOF values confirming that damping identification is more sensitive to severe modal overlap than natural-frequency identification.

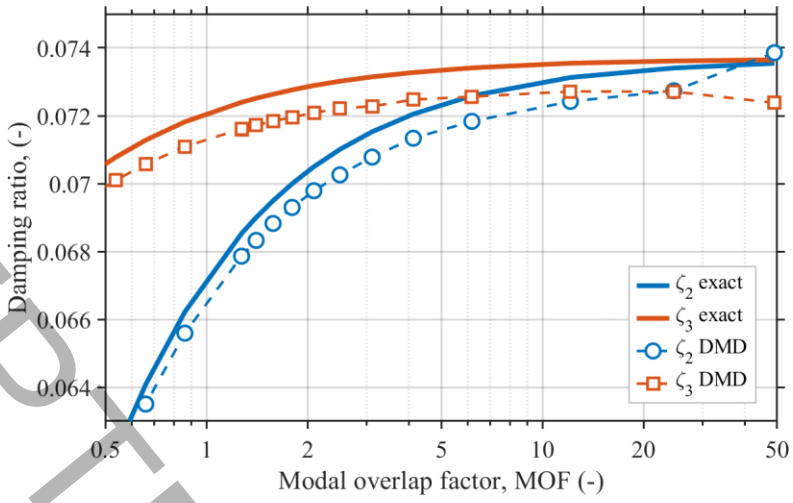


Fig. 14: DMD and reference damping ratios of modes 2 and 3 versus MOF

Fig. 15 shows the natural frequencies estimated by DMD for modes 5 and 6 as a function of MOF. Despite the higher modal order, DMD follows the reference frequencies closely over the full finite MOF range. The frequency errors remain around less than 2%, with only a slight increase as the modal overlap becomes stronger. For the exactly repeated square-plate case, DMD does not separately identify mode 6, consistent with the repeated-eigenvalue condition.

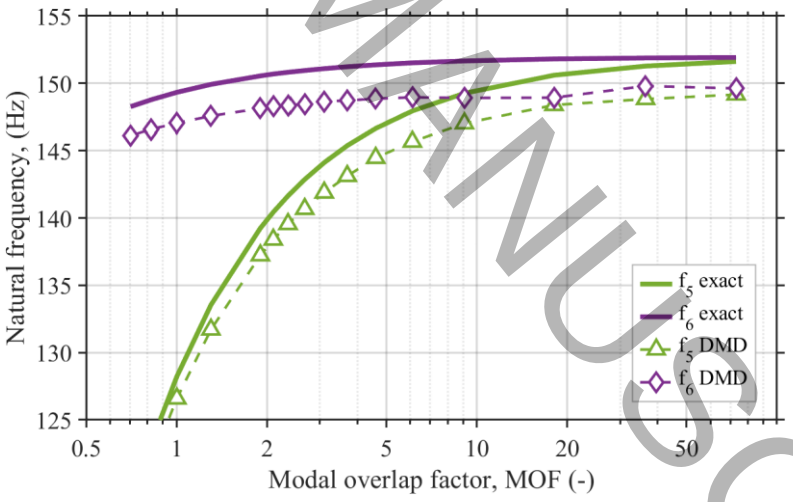


Fig. 15: DMD and reference natural frequencies of modes 5 and 6 versus MOF

Fig. 16 compares the damping ratios estimated by DMD with the reference values for modes 5 and 6 as a function of MOF. Although DMD clearly separates the two modal branches over the investigated finite MOF range, the damping estimates show substantial deviations from the reference values, particularly for mode 6. The errors are considerably larger than those observed for modes 2 and 3 and cannot be regarded as consistently acceptable. These results indicate that, for higher-order closely spaced modes, standard

ACCEPTED MANUSCRIPT

DMD may still distinguish the modal components while providing unreliable damping estimates, especially under strong modal overlap.

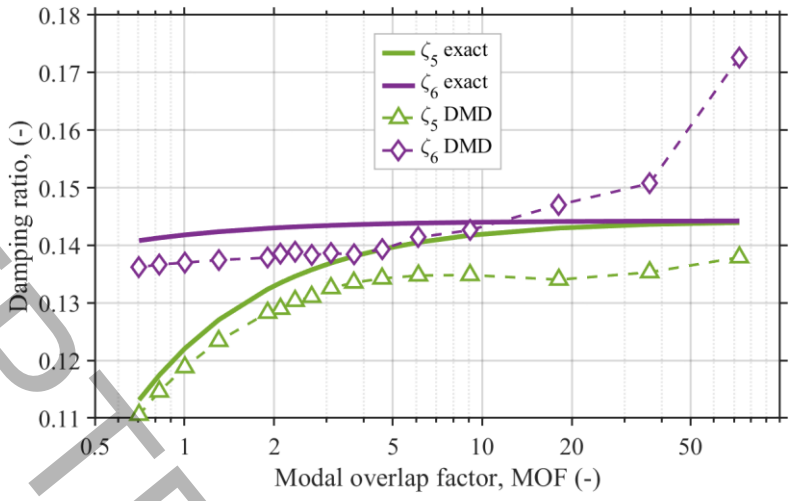


Fig. 16: DMD and reference damping ratios of modes 5 and 6 versus MOF

To examine the estimation errors more clearly, Fig. 17 presents the natural-frequency errors obtained from DMD as a function of MOF. The errors remain small for all identified modes, confirming the high accuracy of standard DMD in estimating closely spaced natural frequencies once the repeated modes are slightly separated. For modes 2 and 3, the error level is almost uniform over the investigated MOF range. In contrast, the errors associated with modes 5 and 6 are slightly larger and show more fluctuations as the modal overlap changes. Nevertheless, the frequency-estimation errors remain below about 2% for all considered finite MOF values, indicating that DMD maintains high accuracy even for the higher-order closely spaced modal pair.

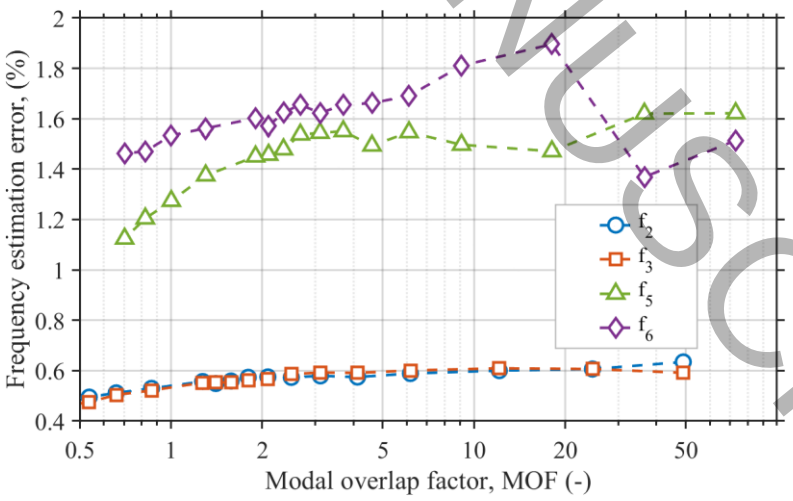


Fig. 17: Error rates for frequency estimation by DMD versus MOF

ACCEPTED MANUSCRIPT

Finally, Fig. 18 presents the damping-ratio errors obtained from DMD as a function of MOF. At relatively low MOF values, the damping ratios are estimated with good accuracy. However, as the modal overlap increases, the errors show larger fluctuations, particularly for the higher-order modes 5 and 6. This behavior is most pronounced for mode 6, where the error increases sharply at the highest finite MOF value. These results indicate that, unlike natural-frequency estimation, damping estimation of higher order modes becomes less accurate under severe modal overlap. This sensitivity may become even more critical in the presence of measurement noise, and therefore the damping estimates under such conditions should be interpreted with caution.

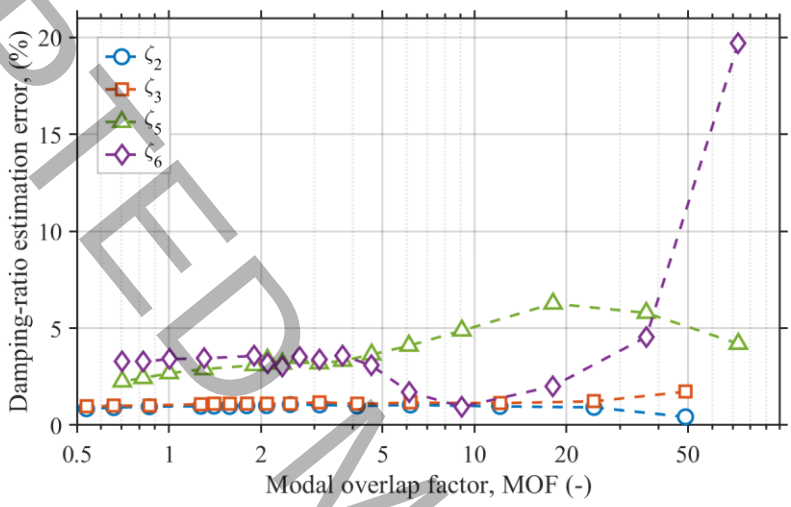


Fig. 18: Error rates for damping ratio estimation by DMD versus MOF

To examine the sensitivity of DMD to the main data-acquisition and numerical parameters, an additional analysis was performed for the higher-order closely spaced modes 5 and 6 of the plate with $b = 402\,\text{mm}$. Record length, sampling frequency, and DMD truncation rank were varied independently, while the remaining parameters were maintained at their baseline values. The baseline condition corresponded to a $T = 0.5\text{s}$ record, sampled at $fs = 2000\,\text{Hz}$, with the full state-space rank retained $r = 162$. The relative errors in the identified natural frequencies and damping ratios with respect to the reference values are summarized in Table 4. N/I indicates that modes 5 and 6 could not be reliably identified as two distinct DMD modes.

Table 4: Sensitivity of DMD estimates to record length, sampling frequency, and truncation rank

Parameter	Value	N	Error f_5 (%)	Error f_6 (%)	Error ζ_5 (%)	Error ζ_6 (%)
Baseline	$T = 0.5\text{s}$ $fs = 2000\,\text{Hz}$ $r = 162$	1001	1.48	1.88	6.28	1.95

ACCEPTED MANUSCRIPT

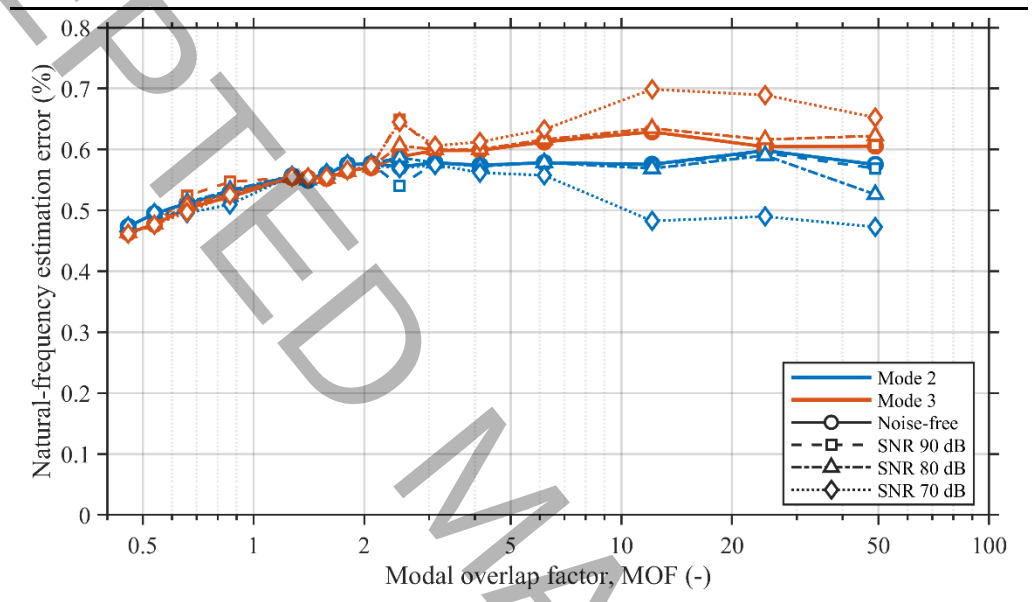
Record Length	$T = 0.2\,\mathrm{s}$	401	1.46	1.97	6.27	1.23
	$T = 0.3\,\mathrm{s}$	601	1.47	1.91	6.27	1.68
	$T = 0.4\,\mathrm{s}$	801	1.48	1.88	6.28	1.92
Sampling Frequency	$fs = 500\,\mathrm{Hz}$	251	N/I	N/I	N/I	N/I
	$fs = 1000\,\mathrm{Hz}$	501	1.54	1.81	3.02	4.41
	$fs = 1500\,\mathrm{Hz}$	751	1.38	1.97	5.32	1.20
DMD rank	$r = 50$	1001	N/I	N/I	N/I	N/I
	$r = 90$	1001	1.29	2.10	7.96	4.79
	$r = 130$	1001	1.63	1.69	6.43	2.04

The results show that the identified natural frequencies are only weakly affected by the investigated data and numerical parameters, with errors remaining approximately within 1.4–2%, whenever both modes are successfully identified. The corresponding damping estimates exhibit greater variability. The limited influence of record length can be attributed to the relatively high modal frequencies, such that even the shortest record of 0.2s contains several oscillation cycles; as illustrated in Fig. 11, more than five cycles are already observable within this interval. In contrast, temporal sampling and rank truncation have a more pronounced effect on the ability of DMD to preserve the two closely spaced modal components. In particular, reducing the rank to 50 does not retain two distinct modes, whereas higher ranks provide paired estimates with varying frequency and damping accuracy. Overall, the results indicate that adequate temporal sampling and sufficient retained rank are more critical than increasing the record length within the investigated range, while damping estimates remain more sensitive than the corresponding natural-frequency estimates.

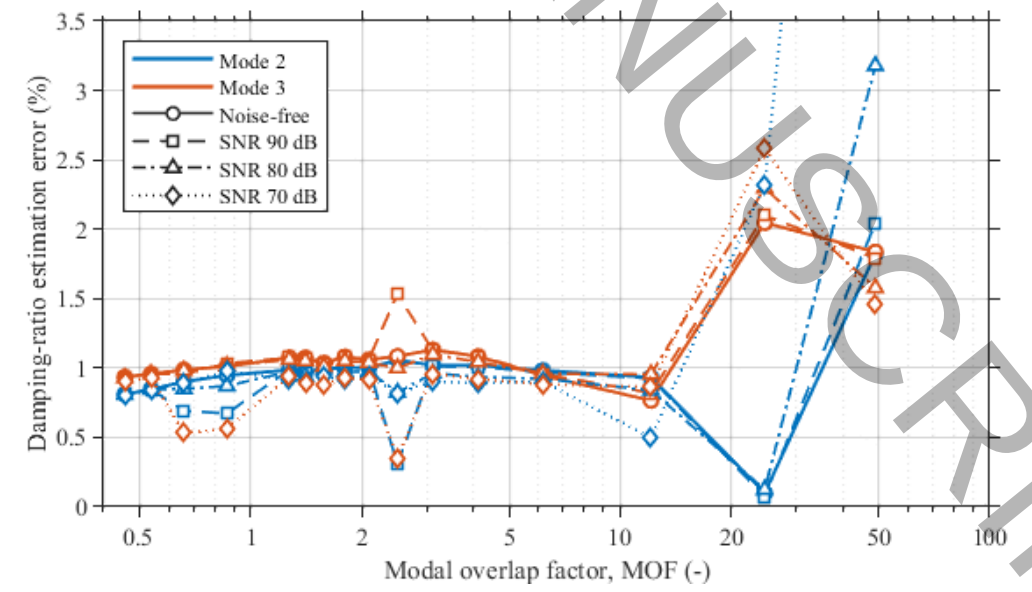
To further assess the robustness of DMD under more practical measurement conditions, the effect of measurement noise was also investigated for the plate model. Similar to the 4-DOF system, random Gaussian noise was added to the response channels at SNR levels of 90, 80, and 70 dB, and the DMD analysis was repeated over 100 realizations. The identified modes were first tracked using their frequency proximity and mode-shape consistency, quantified through the Modal Assurance Criterion (MAC). A modal pair was regarded as successfully resolved when two distinct modal estimates could be identified, both natural frequencies remained sufficiently close to their reference values, and the estimated separation between the two frequencies was also consistent with the reference modal spacing. For the noisy cases, this condition was required to be satisfied in at least 80% of the 100 noise realizations.

ACCEPTED MANUSCRIPT

In this case, rather than presenting the identified modal parameters directly, the estimation errors relative to the reference solutions are plotted as functions of MOF. As shown in Fig. 19(a), the natural-frequency estimates of modes 2 and 3 remain highly accurate over the entire investigated MOF range, with errors consistently below 1% for both the noise-free and noisy datasets. The damping-ratio estimates in Fig. 19(b) are comparatively more sensitive to modal overlap and measurement noise. Nevertheless, the errors remain relatively small over low and moderate MOF values, generally remaining around or below 1–1.5% for $MOF < 20$. Beyond this range, noticeable deviations begin to appear, particularly for mode 2, indicating a reduction in the reliability of damping estimation as the modal overlap becomes more severe.



(a)

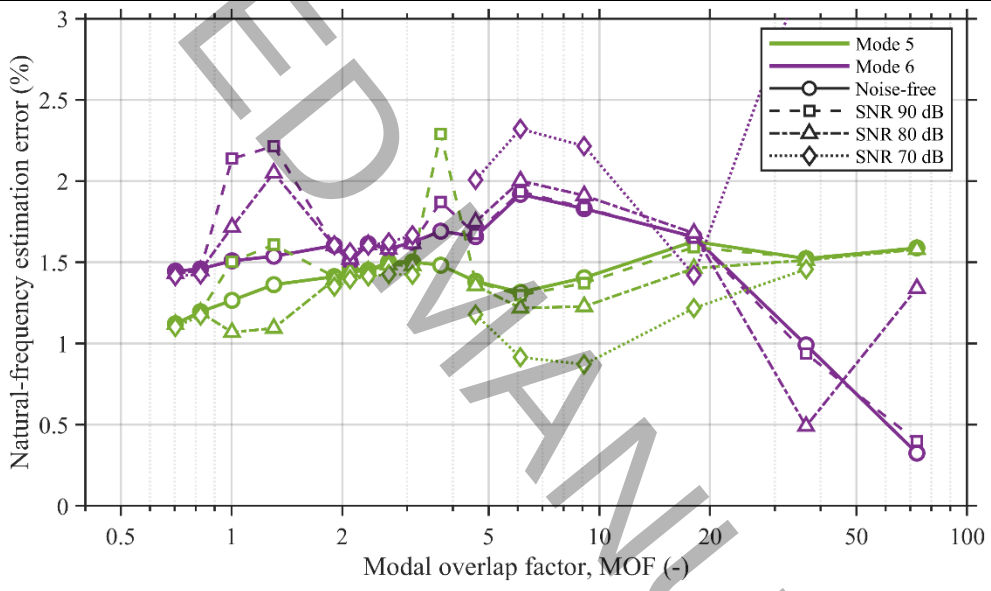


ACCEPTED MANUSCRIPT

(b)

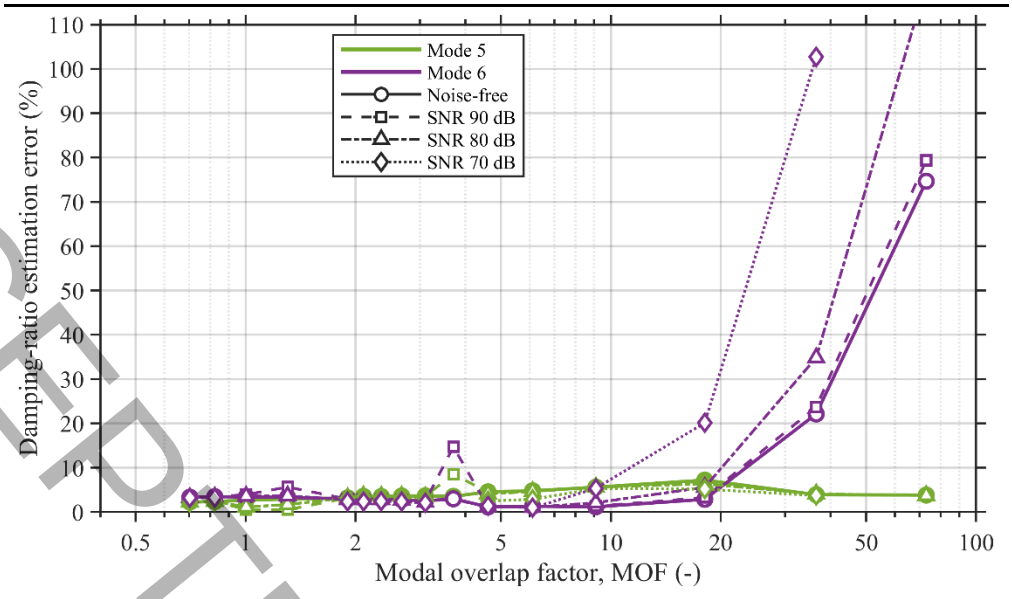
Fig. 19: Noise effect on DMD identification errors for modes 2 and 3: (a) natural-frequency (b) damping-ratio

A similar analysis was performed for the higher-order closely spaced modes 5 and 6, as shown in Fig. 20. The natural-frequency estimates remain comparatively accurate over the investigated MOF range, indicating that DMD can still distinguish the two modal frequencies with relatively small errors even under measurement noise. A different behavior is observed for the damping ratios. At low and moderate modal overlap, the damping estimates remain reasonably accurate; however, beyond a certain MOF, the errors for mode 6 begin to increase markedly. Moreover, the onset of this deviation occurs at progressively lower MOF values as the SNR decreases. This trend indicates that measurement noise reduces the reliable resolution range of the higher-order closely spaced modes, with damping estimation being substantially more sensitive to the combined effects of noise and modal overlap than natural-frequency estimation.



(a)

ACCEPTED MANUSCRIPT



(b)

Fig. 20: Noise effect on DMD identification errors for modes 5 and 6: (a) natural-frequency (b) damping-ratio

To provide an independent benchmark for the resolution capability of DMD, the same response datasets were also analyzed using the well-established Eigensystem Realization Algorithm (ERA). Although reference modal parameters were already available from the finite-element and proportional-damping solutions, ERA was used here as a comparative modal-identification method rather than as a ground-truth reference. For a consistent comparison, both methods were applied to response data with the same sampling frequency, record length, and input-data dimensionality. The number $r = 130$ was selected as DMD truncation rank and the ERA model order was fixed at 40. Table 5 summarizes the maximum resolved MOF values obtained by the two methods under different noise levels. The results show comparable resolution limits under noise-free conditions, whereas ERA generally maintains reliable modal separation over a wider MOF range as the noise level increases. This indicates that, for the present plate model, the resolution capability of DMD is more sensitive to measurement noise, particularly for the higher-order closely spaced modes.

Table 5: Maximum resolved MOF obtained by DMD and ERA under different noise levels

Noise Level	**Mode pair 2,3**		**Mode pair 5,6**	
	DMD	**ERA**	**DMD**	**ERA**
Noise-free	49	49	18	18
$SNR = 90\,\text{dB}$	25	49	18	18
$SNR = 80\,\text{dB}$	25	25	5	18

ACCEPTED MANUSCRIPT

$SNR = 70\,\mathrm{dB}$	6	25	3	9

4. Conclusion

This study quantitatively investigated the resolution capability of standard Dynamic Mode Decomposition for identifying closely spaced and nearly repeated modes in structural systems. Two numerical benchmarks were considered: a previously published 4-DOF benchmark system with controlled stiffness variation and a simply supported plate with variable aspect ratio. A systematic error analysis was performed for the identified natural frequencies and damping ratios, while the influence of modal overlap and measurement noise was also examined.

The results show that DMD can accurately resolve very small frequency separations when a slight split exists between adjacent eigenvalues. In the undamped 4-DOF system, DMD successfully identified nearly repeated modes with a frequency spacing index as small as about 0.01%. In the damped system, the effective resolution range was reduced, although the method continued to provide accurate frequency estimates and useful damping-ratio estimates for closely spaced modes.

The plate example further demonstrated the capability of DMD for both lower- and higher-order closely spaced modes. For modes 2 and 3, the natural frequencies were identified accurately over a wide range of modal overlap. Modes 5 and 6 constituted a more demanding higher-order case, for which DMD was still able to distinguish the two natural frequencies under severe modal overlap. The systematic error analysis showed that natural-frequency estimates were generally more stable than damping-ratio estimates, with the latter becoming increasingly sensitive as the modes approached each other. This sensitivity was particularly evident for the higher-order modal pair.

The noise analysis further clarified the practical limitations of standard DMD. Gaussian measurement noise was introduced at SNR levels of 90, 80, and 70 dB using 100 realizations at each level. Although the natural-frequency estimates remained comparatively stable, the reliable separation of closely spaced modes deteriorated as the noise level increased, and the degradation was more pronounced for the higher-order modes. Comparison with the Eigensystem Realization Algorithm (ERA) showed comparable resolution limits for the noise-free responses, whereas ERA generally maintained reliable modal separation over a wider MOF range under noisy conditions. These results indicate that the principal limitation of standard DMD under severe close-mode conditions is not necessarily the accuracy of the individual frequency estimates, but rather the robustness of modal separation and damping estimation in the presence of measurement noise.

ACCEPTED MANUSCRIPT

The results also confirmed that, in the exact repeated-eigenvalue condition, standard DMD identifies a single temporal eigenvalue for the repeated modal pair rather than separating two independent modes. This behavior should be distinguished from the nearly repeated case, where even a small frequency split can enable the two modes to be identified separately. Overall, standard DMD provides an efficient response-based framework for identifying closely spaced structural modes, with particularly strong performance in natural-frequency estimation, while damping estimation and modal resolution become increasingly sensitive to noise and modal overlap. Future work should therefore focus on experimental validation using measured structural responses and on evaluating noise-robust DMD variants for closely spaced modal identification.

References

[1] A. Agneni, L.B. Crema, G. Coppotelli, Output-only analysis of structures with closely spaced poles, Mechanical systems and signal processing, 24(5) (2010) 1240-1249.
[2] C. Rainieri, G. Fabbrocino, Performance assessment of selected OMA techniques for dynamic identification of geotechnical systems and closely spaced structural modes, Journal of theoretical and applied mechanics, 49(3) (2011) 825-839.
[3] S.H. Kordkheili, S.M. Massouleh, S. Hajirezayi, H. Bahai, Experimental identification of closely spaced modes using NExT-ERA, Journal of Sound and Vibration, 412 (2018) 116-129.
[4] W.-H. Wu, S.-W. Wang, C.-C. Chen, G. Lai, Modal parameter identification for closely spaced modes of civil structures based on an upgraded stochastic subspace methodology, Structure and Infrastructure Engineering, 15(3) (2019) 296-313.
[5] C.-X. Qu, T.-H. Yi, H.-N. Li, B. Chen, Closely spaced modes identification through modified frequency domain decomposition, Measurement, 128 (2018) 388-392.
[6] C. Jonscher, L. Liesecke, N. Penner, B. Hofmeister, T. Grießmann, R. Rolfes, Influence of system changes on closely spaced modes of a large-scale concrete tower for the application to structural health monitoring, Journal of Civil Structural Health Monitoring, 13(4) (2023) 1043-1060.
[7] Y. Kim, L.-q. Chen, Separation of closely spaced modes by combining complex envelope displacement analysis with method of generating intrinsic mode functions through filtering algorithm based on wavelet packet decomposition, Applied Mathematics and Mechanics, 34(7) (2013) 801-810.
[8] T.-H. Le, L. Caracoglia, High-order, closely-spaced modal parameter estimation using wavelet analysis, Structural Engineering and Mechanics, 56(3) (2015) 423-442.
[9] J.-B. Tan, Y. Liu, L. Wang, W.-G. Yang, Identification of modal parameters of a system with high damping and closely spaced modes by combining continuous wavelet transform with pattern search, Mechanical Systems and Signal Processing, 22(5) (2008) 1055-1060.
[10] J.S. Hwang, H. Kim, Mode decomposition of structures with closely distributed modes and nonclassical damping, Structural Control and Health Monitoring, 25(1) (2018) e2065.
[11] C.-S. Lin, System Identification of Structures with Severe Closely Spaced Modes Using Parametric Estimation Algorithms Based on Complex Mode Indicator Function with Singular Value Decomposition, KSCE Journal of Civil Engineering, 24(9) (2020) 2716-2730.
[12] R. Brincker, M. Lopez-Aenlle, Mode shape sensitivity of two closely spaced eigenvalues, Journal of Sound and Vibration, 334 (2015) 377-387.

ACCEPTED MANUSCRIPT

[13] M. Aenlle, J. Pacheco-Chérrez, R. Brincker, Sensitivity analysis of a system with two closely spaced modes using structural dynamic modification, Mechanical Systems and Signal Processing, 206 (2024) 110894.
[14] P.J. Schmid, Dynamic mode decomposition of numerical and experimental data, Journal of fluid mechanics, 656 (2010) 5-28.
[15] A. Saito, T. Kuno, Data-driven experimental modal analysis by dynamic mode decomposition, Journal of Sound and Vibration, 481 (2020) 115434.
[16] C. Wu, Z. Yang, S. He, Efficient modal parameter identification using DMD-DBSCAN and rank stabilization diagrams, Aerospace Science and Technology, 161 (2025) 110112.
[17] C. Wu, S. He, B. Yuan, Z. Yang, An improved NExT-DMD for efficient automated operational modal analysis, Applied Mathematical Modelling, (2026) 116823.
[18] Q. Yang, X. Peng, An exact method for calculating the eigenvector sensitivities, Applied Sciences, 10(7) (2020) 2577.
[19] D. Ruiz, J. Bellido, A. Donoso, Eigenvector sensitivity when tracking modes with repeated eigenvalues, Computer Methods in Applied Mechanics and Engineering, 326 (2017) 338-357.
[20] C.W.R. Jonathan H. Tu, Dirk M. Luchtenburg, Steven L. Brunton, J. Nathan Kutz, On Dynamic Mode Decomposition: Theory and Applications, Journal of Computational Dynamics, 1 (2) (2014) 30.
[21] G. Wang, J. Wu, X. Chen, Y. Du, A sensor signal processing method based on Hankel dynamic mode decomposition, Measurement Science and Technology, 36(3) (2025) 036136.
[22] B.W. Brunton, L.A. Johnson, J.G. Ojemann, J.N. Kutz, Extracting spatial–temporal coherent patterns in large-scale neural recordings using dynamic mode decomposition, Journal of neuroscience methods, 258 (2016) 1-15.
[23] J.-N. Juang, R.S. Pappa, An eigensystem realization algorithm for modal parameter identification and model reduction, Journal of guidance, control, and dynamics, 8(5) (1985) 620-627.
[24] A.S. Phani, J. Woodhouse, Viscous damping identification in linear vibration, Journal of Sound and Vibration, 303(3-5) (2007) 475-500.
[25] D.J. Ewins, Modal testing: theory, practice and application, John Wiley & Sons, 2009.
[26] L. Ljung, System identification, in: Signal analysis and prediction, Springer, 1998, pp. 163-173.

ACCEPTED MANUSCRIPT